Cureus Journal of Agriculture and Food Science
https://doi.org/10.7759/s44497-026-00258-7

Original Article

# Rapid Detection of Deoxynivalenol in Wheat Using 2D Raman Correlation Spectroscopy and Machine Learning

Antony M. Ngugi [1], Zennah C. Kosgey [2], Robinson Ndegwa [3], Jared Ombiro Gwaro [1]

1. *Department of Mathematical and Physical Sciences, Maasai Mara University, Narok, KEN*
2. *Plant Pathology, Kenya Agricultural and Livestock Research Organisation, Nakuru, KEN*
3. *Department of Physics, University of Nairobi, Nairobi, KEN*

Received: March 07, 2026 | Review began: March 30, 2026 | Review ended: August 19, 2026 | Published: September 02, 2026



## Abstract

Fusarium Head Blight (FHB) poses a severe threat to wheat production and food safety in Kenya, leading to significant yield losses and contamination with the mycotoxin deoxynivalenol (DON). Current detection methods are either impractical for field use or lack the sensitivity to detect subsurface toxins. This study developed a rapid detection method by integrating conventional Raman spectroscopy with machine learning algorithms to identify DON-contaminated wheat kernels accurately. FHB symptomatic and healthy wheat heads were collected from farmers' fields, prepared via longitudinal sectioning to expose the endosperm, and analyzed using a portable 785 nm Raman spectrometer. Key spectral bands at 866, 1148, and 1456 $cm^{-1}$ were identified as DON biomarkers through two-dimensional correlation spectroscopy and statistical analysis. Principal Component Analysis (PCA) was employed for dimensionality reduction, with the first 16 principal components accounting for over 95% of the spectral variance. Supervised machine learning models, Support Vector Machine (SVM) and Random Forest (RF), were trained on PCA-transformed data to classify kernels as healthy or infected. The SVM model achieved 97% accuracy, while the RF model attained 100% accuracy on the test set. The entire workflow, from sample preparation to classification, required less than 8 minutes per kernel, demonstrating high throughput potential. The results indicate that conventional Raman spectroscopy, when combined with machine learning, shows potential as a rapid complementary screening approach for detecting DON contamination. With further validation, this method could support improved decision-making in wheat supply chains, particularly in resource-limited settings.

**Categories:** Food quality, Food security and sustainability, Disease & pests of crops

**Keywords:** fusarium head blight, deoxynivalenol, raman spectroscopy, machine learning, wheat kernel classification

## Introduction

Deoxynivalenol (DON), a type B trichothecene mycotoxin, is primarily produced by *Fusarium graminearum* and *Fusarium culmorum*. It is one of the most prevalent contaminants of wheat worldwide. It poses a significant threat to food safety and agricultural sustainability [1,2]. Exposure to DON has been linked to acute gastrointestinal illness, impaired immune response, and reduced livestock productivity, among others. [2]. To mitigate these risks, regulatory agencies have established maximum permissible limits for DON in wheat-based products, with the U.S. Food and Drug Administration (FDA) setting an advisory level of 1 mg/kg (1 ppm) for DON in finished wheat products intended for human consumption [3]. However, surveillance studies in Kenya have reported contamination levels exceeding recommended safety thresholds in major wheat-growing regions [4,5]. These findings highlight the urgent need for rapid, reliable, and locally adaptable monitoring strategies. A central challenge in DON detection lies in its internal accumulation within the

wheat kernel. Following fungal infection, the toxin may localize at depths of approximately 1-3 mm beneath the surface [6], rendering DON itself inaccessible to visual inspection-although visual inspection can identify *Fusarium* infection as an indicator of potential contamination. Conventional detection approaches have significant limitations. Visual grading is rapid and inexpensive but correlates poorly with actual toxin concentration [7]. Immunoassays such as enzyme-linked immunosorbent assays (ELISA) provide faster screening but require destructive extraction procedures and may suffer from antibody cross-reactivity. Confirmatory techniques, including gas chromatography-mass spectrometry (GC-MS), provide excellent sensitivity and specificity. These methods, however, involve labor-intensive sample preparation, expensive equipment, and reliance on centralized laboratories [8]. While near-infrared (NIR) spectroscopy and hyperspectral imaging allow non-destructive screening, their spectral signatures lack the molecular specificity required to uniquely identify DON within the complex biochemical composition of wheat kernels [9,10]. Raman spectroscopy provides molecularly specific information through the vibrational fingerprints of chemical bonds, making it a promising tool for nondestructive chemical analysis [11,12]. Unlike near-infrared methods, Raman scattering reflects molecular structure directly and can differentiate chemically similar compounds [12]. However, Raman signals are inherently weak, and spectra from heterogeneous biological matrices, such as wheat kernels, are challenging to interpret due to overlapping vibrational bands from proteins, starches, lipids, and other endogenous biomolecules [13,14]. This spectral congestion makes it difficult to detect contributions from low-level contaminants such as DON, especially when present at trace concentrations relative to the dominant matrix components [15,16]. These interpretative challenges have been widely reported in food and biological systems, highlighting the need for chemometric tools [12-14]. Spectral preprocessing, targeted feature extraction, and multivariate statistical analyses are essential to enhance signal discrimination and detect trace-level toxins with confidence [15,16].

Early applications of Raman spectroscopy in wheat primarily aimed to detect *Fusarium* fungal infection rather than directly measure DON concentrations [17,18]. To improve sensitivity for trace-level toxin detection, enhanced techniques such as surface-enhanced Raman spectroscopy (SERS) have been introduced, achieving lower detection limits through nanoparticle-assisted signal amplification [19, 20]. However, SERS protocols typically require multi-step substrate preparation, controlled nanoparticle synthesis, and careful optimization, which complicate standardization and hinder practical field deployment [19,20]. Many validation studies employ artificially spiked samples instead of naturally infected wheat, limiting the assessment of method performance under realistic contamination conditions [21,22]. Spatially Offset Raman Spectroscopy has also been explored to probe subsurface layers of wheat kernels, but its application depends on specialized optical configurations and expensive instrumentation, making routine screening in resource-limited settings impractical [23]. Finally, predictive models reported in the literature are often trained on artificially inoculated wheat or cultivars from temperate regions, which may not adequately capture the infection dynamics and environmental variability of tropical agro-ecosystems [18,24]. Collectively, these limitations underscore the absence of a rapid, portable, and molecular-specific method validated on naturally infected wheat from tropical production regions. In this study, we integrated portable 785 nm Raman spectroscopy with two-dimensional correlation spectroscopy (2D-COS) to enhance spectral resolution and identify co-varying vibrational features associated with DON [25]. Characteristic bands at 866, 1148, and 1456 $cm^{-1}$ were used to construct targeted feature sets for classification via Support Vector Machine (SVM) and Random Forest (RF) algorithms. Models were validated against quantitative immunoassay measurements. The approach was evaluated on naturally infected wheat samples from Kenya, with an analysis time of less than 8 minutes per kernel, demonstrating its potential as a rapid complementary screening approach for local grain supply chains, subject to further validation.

## Materials And Methods

### Sample collection and preparation

Wheat (*Triticum aestivum L.*) kernels naturally infected with FHB were collected from the Kenya Agricultural and Livestock Research Organization research farm in Njoro, Nakuru County, Kenya, rather than from commercial manufacturers, ensuring traceable provenance from documented occurrence of *Fusarium* species [26]. Harvesting of the symptomatic and healthy wheat heads was conducted during the 2025 growing season, planted in March and harvested in September,

**How to cite this article:**
Ngugi A M, Kosgey Z C, Ndegwa R, et al. (September 02, 2026) Rapid Detection of Deoxynivalenol in Wheat Using 2D Raman Correlation Spectroscopy and Machine Learning. Cureus J. Agri. Food Sci 2 : es44497-026-00258-7. DOI https://doi.org/10.7759/s44497-026-00258-7

and grains were immediately transported to the laboratory in sealed, sterile containers to prevent post-collection contamination and moisture loss. Once in the lab, samples were air-dried at ambient temperature (22-25°C) to stabilize metabolic activity and minimize further fungal growth. Visual inspection was performed under controlled white LED illumination (10,000 lux) following established FHB grading protocols [6].

Each kernel was individually examined using sterile forceps and categorized based on morphological and pigmentation characteristics. The total dataset comprised 70 kernels, which were prepared for spectroscopic analysis. From these, 195 spectra were acquired (approximately 3 spectra per kernel) and selected for machine learning model development, ensuring balanced representation of visually healthy and infected categories. To overcome limitations associated with whole-kernel Raman acquisition, including surface curvature effects, pericarp-induced fluorescence, and poor spectral reproducibility, a longitudinal sectioning protocol was implemented. Each kernel was positioned on a sterile glass slide and carefully split along its length using a surgical scalpel, exposing the homogeneous endosperm surface. This preparation method minimized fluorescence background, enhanced spectral consistency, and provided direct access to the tissue where DON accumulation predominantly occurs [7]. While Raman measurements themselves are non-destructive, the longitudinal sectioning step used in this study is destructive.

### Raman spectra acquisition

Raman spectra were acquired using a portable EZRaman NP 785 spectrometer (Enwave Optronics, USA) equipped with a 785 nm excitation laser, which was selected to minimize autofluorescence interference, a known challenge in plant tissue analysis [27]. The instrument was calibrated before each measurement session using a polystyrene reference standard. Spectra were recorded over the 200-2000 $cm^{-1}$ range with a spectral resolution of 1.290 $cm^{-1}$. Optimized acquisition settings consisted of a laser power of 300 mW, an integration time of 5 seconds per scan, and 5 averaged scans per spectrum. To account for sample heterogeneity and ensure reproducible spectral collection, three spectra were collected from random positions on each longitudinally sectioned kernel. All measurements were performed in a darkened environment at ambient temperature to eliminate ambient light interference, and spectral intensities were normalized to a 0-1 scale to enable consistent comparative analysis. Raw Raman spectra were preprocessed using Python to correct for fluorescence background, noise, and spikes. 2D-COS was applied to identify coherent spectral variations associated with DON contamination. Synchronous 2D-COS maps were generated following the methodology of Ndung'u et al. [25], using the mean spectrum of healthy kernels as the reference. Correlation intensities were normalized to a 0-1 scale and visualized as contour plots with 40 evenly spaced levels. Regions exhibiting strong autopeaks, indicating synchronous intensity changes across samples, were extracted as candidate biomarkers for DON.

To validate the non-destructive Raman classifications, a subset of kernels was subjected to quantitative DON analysis using the AgraVision™ Reader system. Following Raman acquisition, each kernel was individually processed for quantitative DON analysis using the AgraVision Reader. The kernels were ground to a fine powder using a mortar and pestle and homogenized. A 10 g aliquot of each powdered sample was mixed with 50 mL of distilled water (1:5 w/v), shaken vigorously for 2 minutes, and filtered through Whatman No. 1 filter paper. The filtrate was applied to AgraVision™ test strips following the manufacturer's protocol. DON concentrations were recorded in parts per billion (ppb) within 5-10 minutes of application. These values provided an independent, quantitative reference against which Raman spectral features were calibrated.

### Machine learning model development and evaluation

To reduce dimensionality and extract informative features from the preprocessed spectral dataset, PCA was performed. The first 16 principal components (PCs), which collectively represented over 95% of the total variance, were selected as input features for the subsequent classification tasks. To avoid data leakage, the PCA transformation was derived solely from the training data. This fitted transformation was subsequently used to process both the training and test sets, ensuring that the test set did not influence the dimensionality reduction process. These PCs effectively captured the main spectral variations linked to biochemical changes in infected kernels. For the classification step, two supervised learning

**How to cite this article:**
Ngugi A M, Kosgey Z C, Ndegwa R, et al. (September 02, 2026) Rapid Detection of Deoxynivalenol in Wheat Using 2D Raman Correlation Spectroscopy and Machine Learning. Cureus J. Agri. Food Sci 2 : es44497-026-00258-7. DOI https://doi.org/10.7759/s44497-026-00258-7

algorithms, RF and SVM were chosen. These models are well-regarded for their strong performance in analyzing high-dimensional spectroscopic data and their ability to capture complex, nonlinear relationships between spectral inputs and target classes [28,29]. All models were developed using the Python scikit-learn library (version 1.3.0).

The RF classifier was built as an ensemble of decision trees. Each tree was trained on a bootstrap sample drawn from the original training data, a technique that promotes diversity among the individual models [30]. At each node split, a random subset of predictor variables specifically, the square root of the total feature count was evaluated. This random feature sampling helps decorrelate the trees and improves the model's capacity to generalize to new, unseen data. The final classification output was determined by a majority vote, aggregating the predictions from all T = 200 trees. Node splits were guided by the Gini impurity metric, which quantifies the purity of class labels within each node.

The SVM was also implemented using an RBF kernel with C = 1.0 and γ = 'scale', using the default scikit-learn scaling rule for γ. This method is designed to find the optimal separating hyperplane between classes [31]. For datasets that are not linearly separable in their original feature space, the RBF kernel maps the samples into a higher-dimensional space where a linear separation can be achieved. The kernel is expressed as:

$$K(x_i, x) = \exp\left(-\gamma \|x_i - x\|^2\right) \tag{1}$$

where γ controls the influence of individual training samples on the decision boundary.
The classification of a new sample is then given by:

$$f(\mathbf{x}) = \text{sign}\left(\sum_{i=1}^{n} \alpha_i y_i K(\mathbf{x}_i, \mathbf{x}) + b\right) \tag{2}$$

with αi representing the Lagrange multipliers obtained from the optimization process, yi $\in$ {−1, +1} the class labels, and b the bias term. The SVM optimization problem balances two competing objectives: maximizing the margin (minimizing $\|$ w $\|$ 2) and minimizing classification errors on the training data. This trade-off is controlled by a regularization parameter C, which penalizes misclassified samples [32]. The final dataset comprised 195 spectra, which were divided into training and test subsets using a 80/20 split. Stratification was employed to maintain the original class proportions in both subsets. In addition to this single split, model robustness was evaluated through 5-fold stratified cross-validation. Here, the data were randomly divided into five equal parts; each part served as a validation set once, while the remaining four were used for training. This process was repeated five times, and the average performance metrics along with their standard deviations were calculated to obtain a more reliable estimate of how well the models would generalize to new data. After model training, performance was measured on the withheld test set. The evaluation relied on metrics derived from the confusion matrix, which records true positives (TP), true negatives (TN), false positives (FP), and false negatives (FN). The following metrics were used:

$$\text{Accuracy} = \frac{TP + TN}{TP + TN + FP + FN} \tag{3}$$

$$\text{Precision} = \frac{TP}{TP + FP} \tag{4}$$

$$\text{Recall} = \frac{TP}{TP + FN} \tag{5}$$

$$\text{F1-Score} = 2 \times \frac{\text{Precision} \times \text{Recall}}{\text{Precision} + \text{Recall}} \tag{6}$$

Accuracy gives an overall sense of the proportion of correctly classified samples. Precision reflects the reliability of positive predictions: how many of the samples labeled as positive actually belong to the positive class. Recall, also known as sensitivity, indicates the model's ability to correctly identify all actual positive cases. The F1-score, being the harmonic mean of precision and recall, provides a balanced performance measure that is especially useful when the class

distribution is imbalanced [33-35]. Additionally, receiver operating characteristic (ROC) curves were constructed, and the area under the ROC curve was computed to assess the discriminative power of each classifier across various threshold settings. All computational steps were executed in Python (version 3.9). Statistical analyses, including on e-way analysis of variance (ANOVA) and post-hoc Tukey HSD tests, were conducted using the SciPy (version 1.11.0) and statsmodels (version 0.14.0) libraries.

## Results And Discussion

### Raman spectral analysis of healthy and *Fusarium*-infected wheat samples for deoxynivalenol detection

The averaged Raman spectra of healthy wheat kernels, *Fusarium*-infected kernels, and pure DON standard are presented in Figure *1* across the 400-1800 $cm^{-1}$ fingerprint region. Healthy kernels exhibited broad, low-intensity bands primarily reflecting native starch and protein vibrations typical of uninfected endosperm tissue. However, infected kernels displayed sharp increases at specific wavenumbers: 860-870 $cm^{-1}$, 1140-1155 $cm^{-1}$, and 1450-1465 $cm^{-1}$. These same bands appeared with even greater intensity in the pure DON reference spectrum, providing strong qualitative evidence that *Fusarium* infection results in direct deposition and accumulation of DON within the grain matrix.

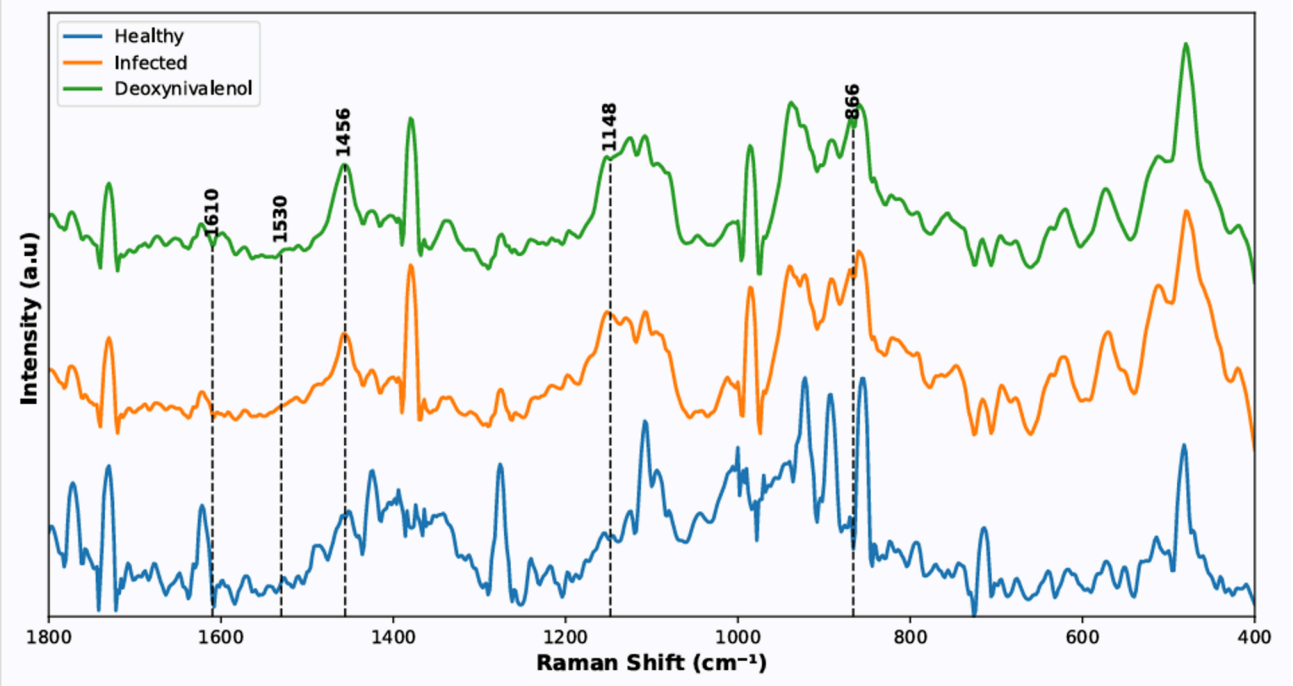


**FIGURE 1: Representative average Raman spectra of healthy wheat, infected wheat, and the deoxynivalenol standard**

The band near 860-870 $cm^{-1}$ corresponds to trichothecene ring-breathing and C-O-C deformation modes, which are central to DON's molecular structure [19,21]. The most widely reported DON marker in Raman and SERS studies the band near 1450-1465 $cm^{-1}$ was observed and assigned to CH and CH2 deformations of the trichothecene backbone [20,22]. Higher-frequency features near 1530-1610 $cm^{-1}$ were also present in both infected and DON spectra, though weaker. These bands have been associated with C=C stretching in DON's alternating double-bond system [21,36]. Their consistent co-occurrence alongside the core DON bands reinforces the interpretation that the observed changes originate from

trichothecene contamination rather than nonspecific matrix variation. Similar patterns have been documented in prior Raman and SERS studies of contaminated cereals [19,20], further supporting the conclusion that the observed Raman bands are characteristic of DON specifically, rather than arising from non-specific biochemical changes in infected wheat.

**Two-dimensional correlation spectroscopy (2D-COS) analysis**

2D-COS was applied to identify Raman bands exhibiting the most significant changes between healthy and DON-contaminated wheat kernels, and to assess whether spectral variations at DON-associated frequencies were coherent across samples. This approach is critical because positive synchronous correlations reveal in-phase spectral changes, indicating that a chemical perturbation affects several vibrational modes simultaneously [37]. The synchronous 2D-COS map in Figure *2* was generated by comparing spectra from samples above and below the DON contamination threshold. Following Noda's rules, diagonal auto-peaks represent spectral regions where intensities change systematically with increasing DON concentration. The map shows three dominant diagonal auto-peaks at 866, 1148, and 1456 $cm^{-1}$. These bands exhibited the strongest systematic intensity variations across the dataset, confirming that they respond consistently to DON presence in wheat kernels. The warm colors (red-to-yellow) along the diagonal indicate strong positive self-correlations, meaning these features are consistently present in contaminated samples.

According to Noda's theory, diagonal features represent self-correlations, and strong positive values signify that these intensities increase together as the perturbation in this case, fungal infection and DON accumulation intensifies [38]. This behavior is chemically meaningful: DON's trichothecene framework contains coupled ring, C-O, and CH-deformation vibrational units, explaining why the spectral enhancements in the 866, 1148, and 1456 $cm^{-1}$ regions occur simultaneously [22,39]. Off-diagonal cross-peaks, while less prominent in this region, would indicate interactions between different vibrational modes, further demonstrating DON's influence on the biochemical profile of wheat kernels. 2D-COS confirmed that these bands responded coherently to infection, with synchronous correlations demonstrating that all three intensities increase simultaneously as DON accumulation progresses [37,38]. The close agreement between the infected wheat spectra and the pure DON standard provides compelling evidence that the observed spectral changes are directly attributable to DON accumulation rather than secondary infection effects.

**How to cite this article:**
Ngugi A M, Kosgey Z C, Ndegwa R, et al. (September 02, 2026) Rapid Detection of Deoxynivalenol in Wheat Using 2D Raman Correlation Spectroscopy and Machine Learning. Cureus J. Agri. Food Sci 2 : es44497-026-00258-7. DOI https://doi.org/10.7759/s44497-026-00258-7

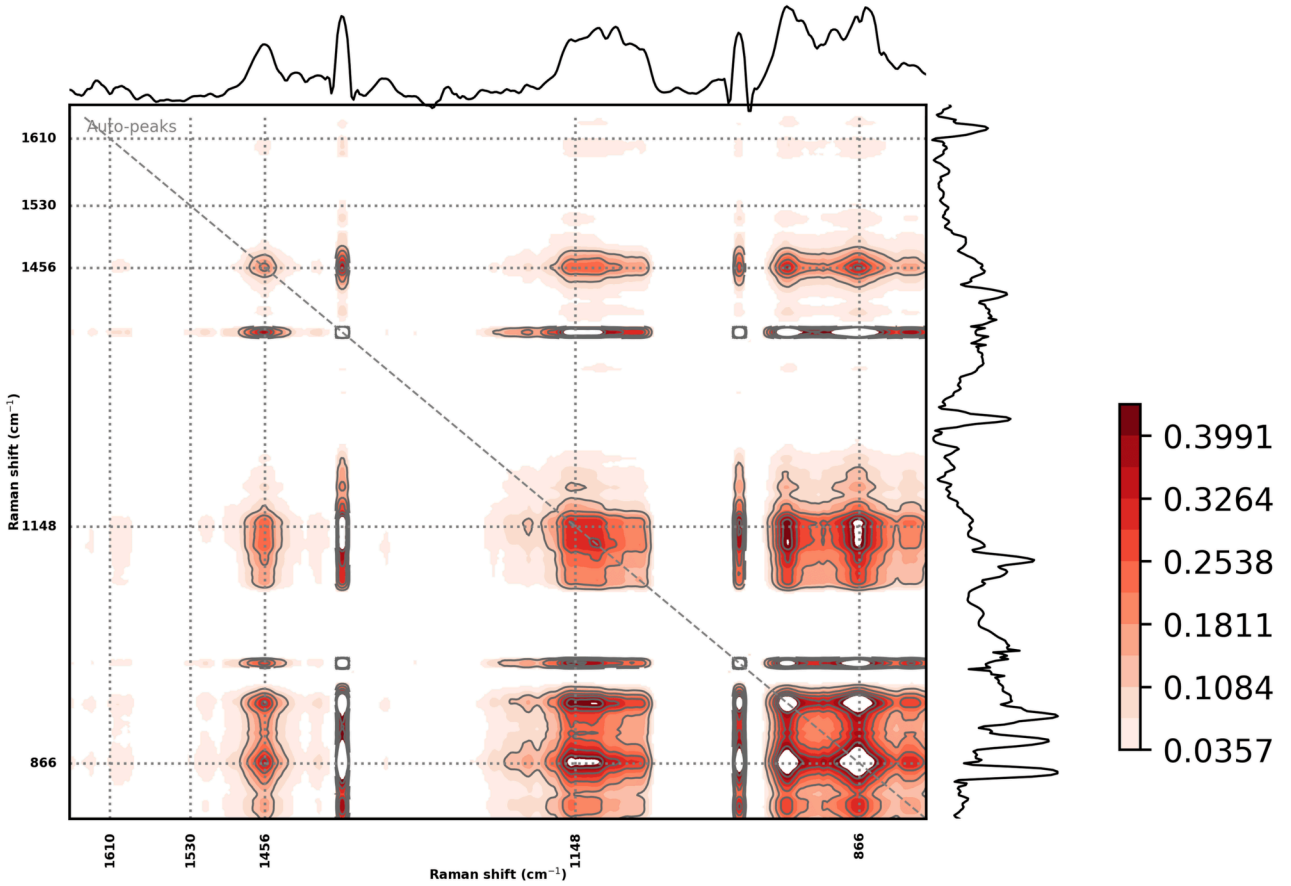


**FIGURE 2: Synchronous 2D-COS Raman map of wheat kernels (800–1650 cm−1). Prominent auto-peaks appear at 866, 1148, and 1456 cm−1, with warmer colors indicating stronger positive correlations. The top and right margins display the corresponding mean spectra for the infected and control samples, respectively**

2D-COS, Two-Dimensional Correlation Spectroscopy

### Chemometric classification via PCA

To verify whether these spectral variations drive sample clustering, PCA was performed on the 860-1650 $cm^{-1}$ region, which contains all three 2D-COS peaks. The PCA scores plot (Figure *3*) shows a clear progression from healthy wheat to infected kernels and finally to pure DON along PC1. The first two PCs explained a substantial portion of the variance: PC1 = 59.4%, PC2 = 10.0%. This pattern indicates that the same DON-related bands dominating the 2D-COS map also explain the largest source of variance in the dataset. The close agreement between the two methods confirms that these frequencies carry the dominant chemical information associated with DON contamination. Restricting PCA to the 2D-COS-identified window (860-1650 $cm^{-1}$) enabled clear separation of healthy, infected, and pure DON samples. This aligns with observations by [40] who noted that limiting analysis to chemically meaningful vibrational regions improves discrimination compared to using the entire Raman spectrum. PCA further validated these findings by clearly separating healthy, DON standard and infected samples along the first PC, which alone explained nearly 60% of the total variance.

**How to cite this article:**
Ngugi A M, Kosgey Z C, Ndegwa R, et al. (September 02, 2026) Rapid Detection of Deoxynivalenol in Wheat Using 2D Raman Correlation Spectroscopy and Machine Learning. Cureus J. Agri. Food Sci 2 : es44497-026-00258-7. DOI https://doi.org/10.7759/s44497-026-00258-7

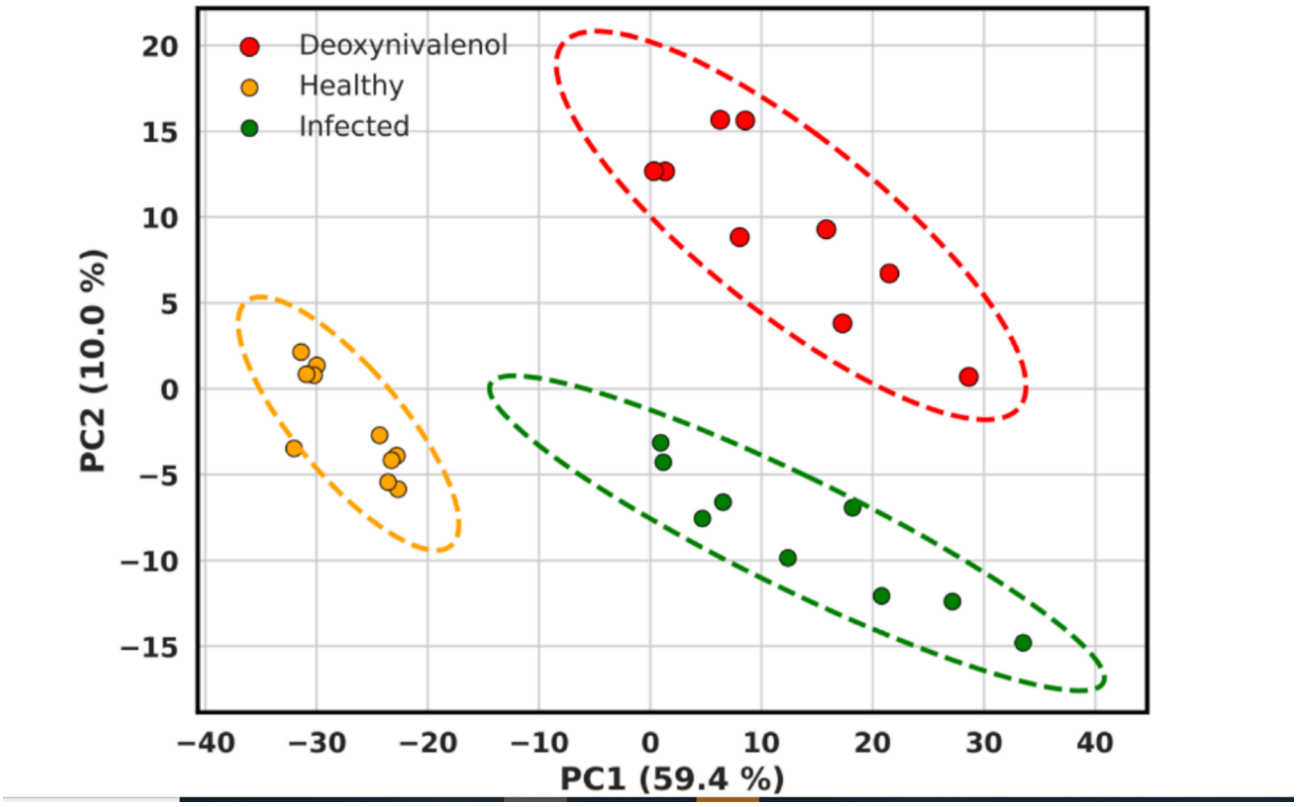


**FIGURE 3: PCA score plot for the regions identified by 2D-COS**

PCA, Principal Component Analysis; 2D-COS, Two-Dimensional Correlation Spectroscopy

### Combined-mean analysis of DON-related Raman peaks using laboratory reference concentrations

The combined-mean analysis Figure *4* presents the average intensity of the three DON-related Raman peaks 866, 1148, and 1456 $cm^{-1}$ across the Healthy, DON standard, and Infected wheat samples. By averaging these peaks, the plot captures the overall spectral response associated with DON contamination, providing a single representative value for each sample. The resulting distribution shows a clear, progressive increase in mean intensity from Healthy to DON standard and Infected samples, reflecting the laboratory reference concentrations of 0.0, 1.78, and 2.3 ppm, respectively. Healthy kernels clustered at the lowest combined mean intensities, consistent with the absence of detectable DON; the DON standard formed an intermediate group; and Infected samples displayed the highest values, mirroring the expected contamination gradient. This combined approach confirms that the collective behavior of the three selected Raman peaks reliably tracks increasing DON levels. The averaging reduces variability from individual peaks, providing a visual summary of spectral separation among the sample groups and supporting the use of these characteristic peaks for subsequent quantitative and classification analyses. One-way ANOVA confirmed significant differences in mean peak intensities (866, 1148, and 1456 $cm^{-1}$) among healthy, DON standard, and infected groups ($p < 0.001$). Post-hoc Tukey HSD tests revealed that all pairwise comparisons were statistically significant ($p < 0.05$), confirming that the spectral markers reliably discriminate between contamination levels. The combined-mean intensity analysis showed a progressive increase from healthy (0.0 ppm) to DON standard (1.78 ppm) to infected samples (2.3 ppm), strengthening the causal link between spectral features and DON concentration.

**How to cite this article:**
Ngugi A M, Kosgey Z C, Ndegwa R, et al. (September 02, 2026) Rapid Detection of Deoxynivalenol in Wheat Using 2D Raman Correlation Spectroscopy and Machine Learning. Cureus J. Agri. Food Sci 2 : es44497-026-00258-7. DOI https://doi.org/10.7759/s44497-026-00258-7

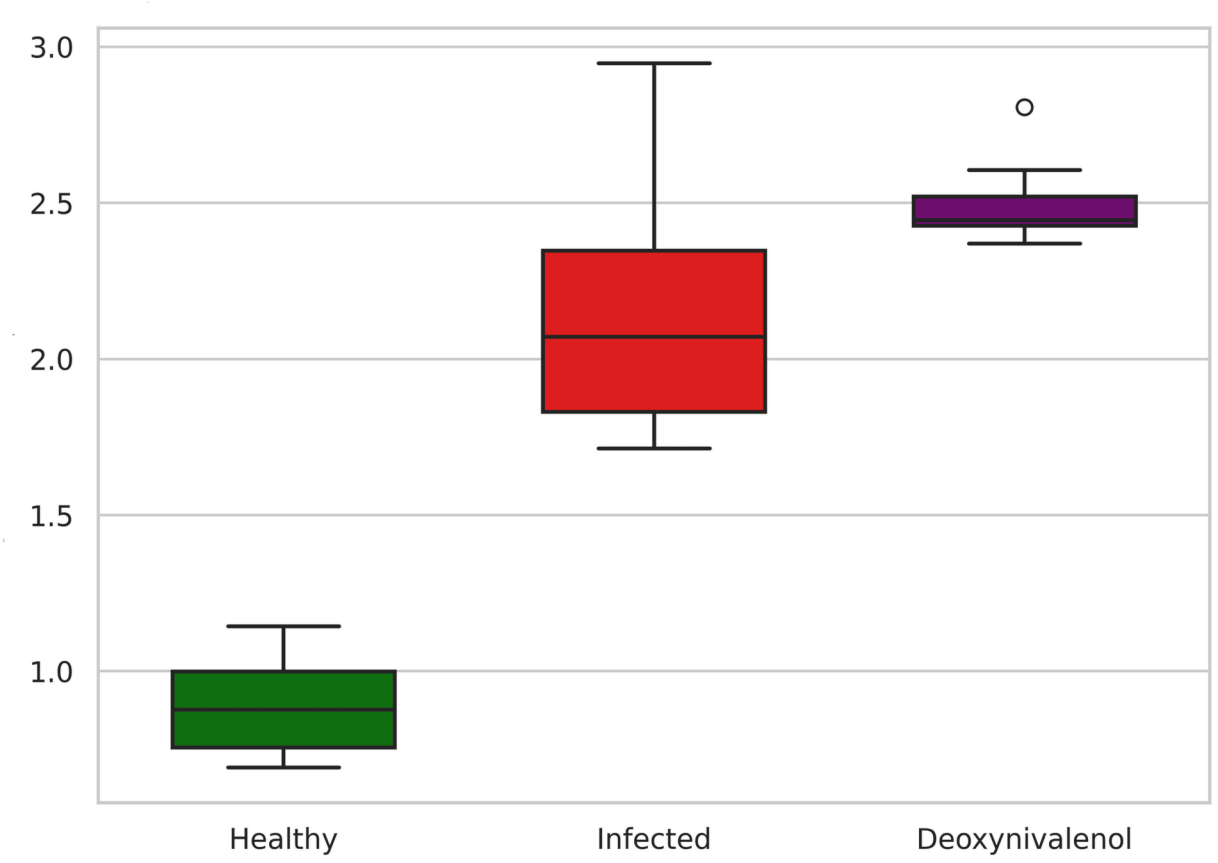


**FIGURE 4: Combined mean Raman intensities of the three characteristic DON-related peaks (866, 1148, and 1456 cm−1) across Healthy, DON standard, and Infected wheat samples**

DON, Deoxynivalenol

### Classification performance using identified DON spectral markers

The SVM classifier with an RBF kernel was trained using 16 PCs derived from the DON-sensitive spectral region. Sixteen PCs were selected because this number captured over 95% of the total cumulative variance, as shown in Figure *5*. The selection of 16 PCs was based on the cumulative explained variance, which exceeded 95%. Retaining components that explain 90-95% of the total variance is a standard practice in chemometric analysis of spectroscopic data, as it balances the retention of chemically relevant information with the reduction of noise [41]. This approach has been widely applied in Raman and near-infrared studies of agricultural products to ensure robust dimensionality reduction. The resulting classification was robust: out of 39 total tests samples, 21 healthy kernels and 17 infected kernels were correctly classified, with only one sample misclassified. This yielded an overall accuracy of 97%, with correspondingly high sensitivity and specificity (Figure *6*). The precision and recall for each class ranged between 0.95 and 1.00, indicating that both false negatives and false positives were essentially negligible. The single misclassification suggests that the model is not overfitting and has genuine predictive power, although larger sample sets would be needed to confirm stability.

To complement the SVM model and strengthen classifier reliability, a RF classifier was also trained using the same 16 PCA-derived components. In the test set of 60 samples that was not used for training, the RF model was found to be 100% accurate for the independent test set, correctly identifying all 21 healthy and 18 infected kernels (Figure *7*). To assess model stability more rigorously, 5-fold stratified cross-validation was performed on the entire dataset. The RF model

achieved a mean cross-validation accuracy of 98.2% (±1.1%), with corresponding precision and recall values of 0.98 (±0.02) for both classes. The low standard deviation at the different folds suggests consistency across folds and minimal data partition dependency. Furthermore, the models were trained using only the first 16 PCs and the 2D-COS-selected spectral region, instead of the high-dimensional spectrum. The targeted feature selection means that the possibility of fitting noise is decreased. While the high test-set accuracy is encouraging, the relatively small dataset size means that further external validation on independent samples from different locations and wheat varieties is necessary to confirm the generalizability of the models.

Figure *7* shows a perfect diagonal with zero misclassifications. Results obtained from these classifications are in line with the balanced sampling strategy described in the Sample Collection and Preparation subsection, where strict care was taken to sample kernels and to collect spectra to reduce pseudo-replication and to ensure coverage of both the healthy and infected classes. The accuracy observed is very good and is a true reflection of the controlled provenance of the data, being kernels from a single research farm. This provides some validation of the robustness of the DON-specific spectral separation but additional validation with a wider range of sources and contamination levels will be needed before it can be generalized.

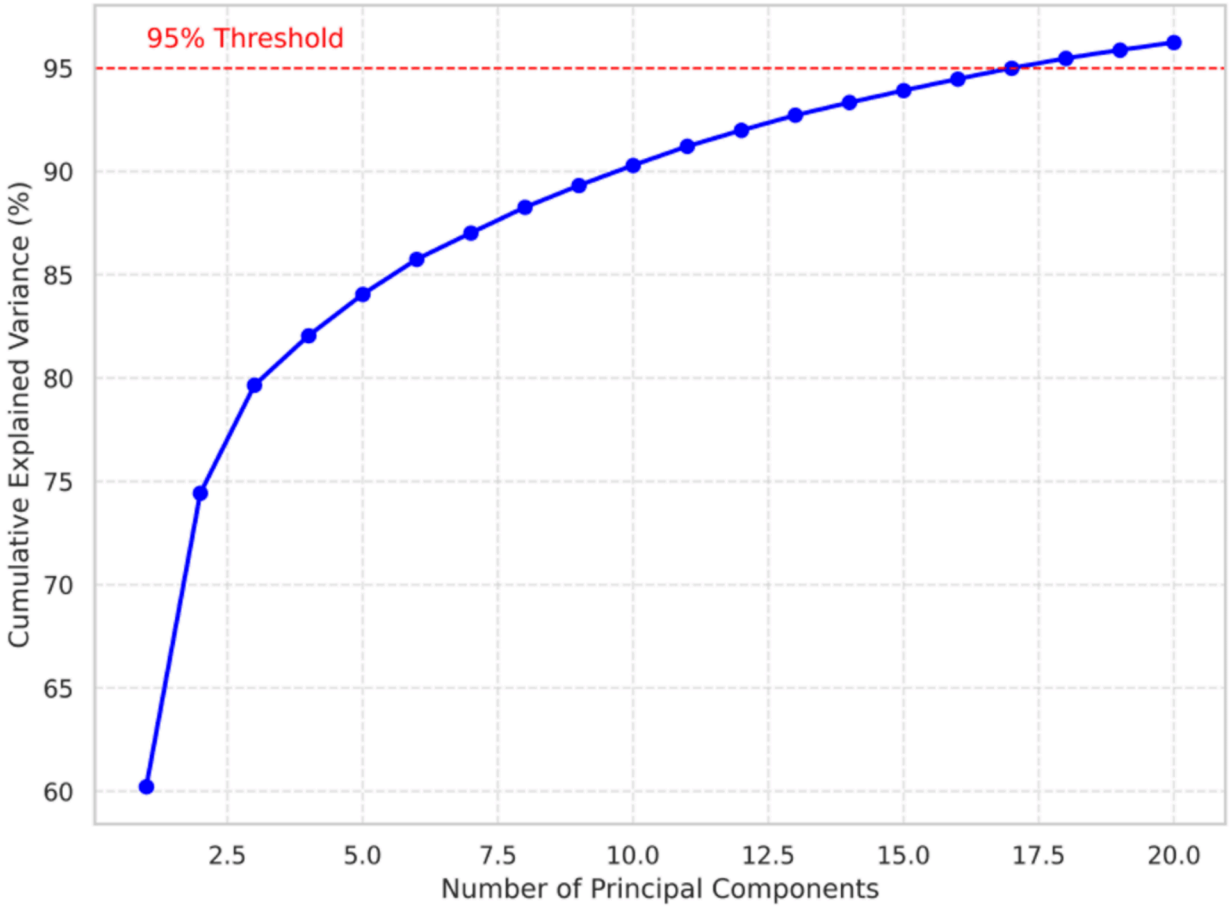


**FIGURE 5: Cumulative variance of principal components the red line indicates the 95% threshold. The first 16 PCs account for over 95% of total variance**

PC, Principal Component

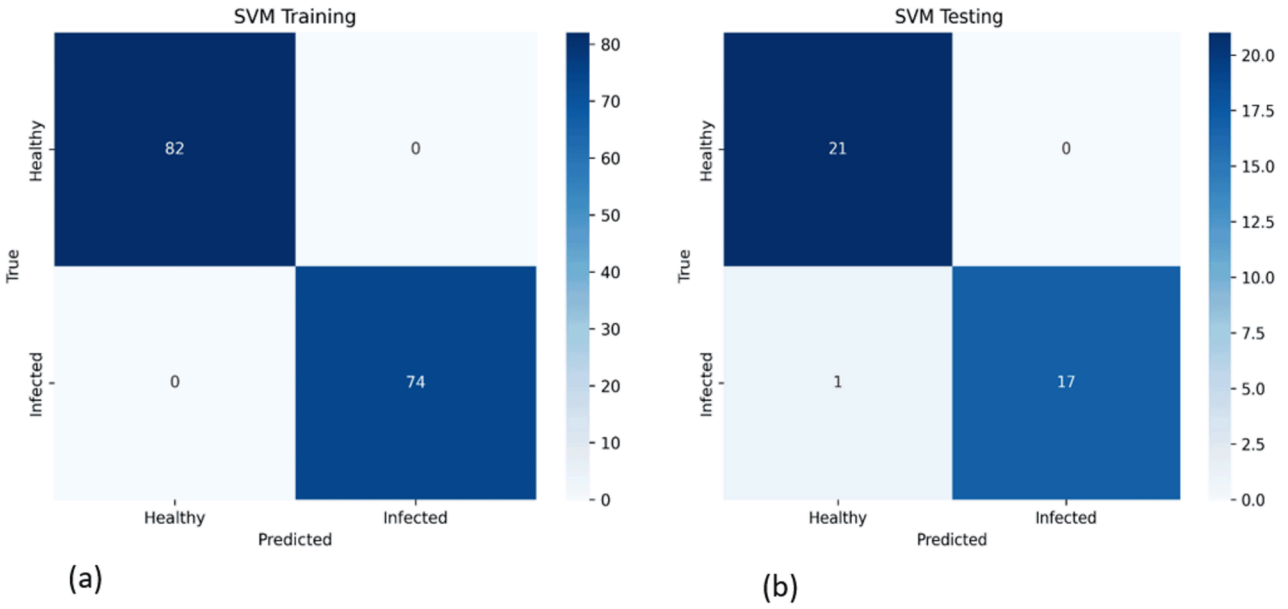


**FIGURE 6: Confusion matrices for SVM model. Panels (a) and (b) show training set and test set results, respectively**

SVM, Support Vector Machine

This complete separation demonstrates that RF, which leverages ensemble decision trees and bootstrap aggregation, effectively captures discriminatory features within the DON-sensitive spectral region. The perfect precision, recall, and F1-scores for both classes (1.00 each) reinforce the conclusion that the selected PCA components carry a strong chemical signal that is readily learned by an ensemble classifier. The excellent RF performance is consistent with current literature, where RF models have demonstrated high robustness and stability in spectroscopic and food-contaminant detection tasks due to their ability to handle correlated variables and non-linear patterns [40].

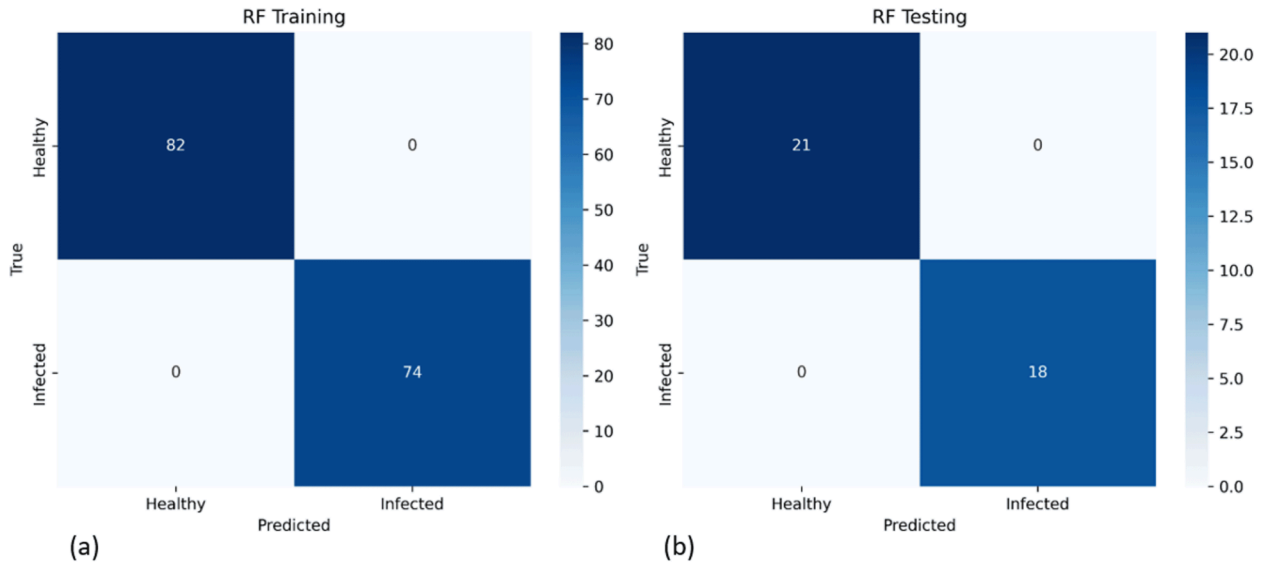


**FIGURE 7: Confusion matrices for Random Forest model. Panels (a) and (b) show training set and test set results, respectively**

| Model | Class | Precision | Recall | F1-Score | Test Set Accuracy | CV Accuracy (Mean ± Std) |
|---|---|---|---|---|---|---|
| SVM | Healthy<br>Infected | 0.95 1.00 | 1.00 0.94 | 0.98 0.97 | 0.97 | 0.96 ± 0.02 |
| RF | Healthy<br>Infected | 1.00 1.00 | 1.00 1.00 | 1.00 1.00 | 1.00 | 0.98 ± 0.01 |

**TABLE 1: Performance metrics for SVM and Random Forest classifiers**

SVM, Support Vector Machine

The performance metrics for both models are summarized in Table *1*. Supervised machine learning classification achieved high diagnostic accuracy, with the SVM model reaching 97% accuracy and the RF model achieving perfect 100% classification on the test set. The good performance of RF may be attributed to its ensemble nature, which effectively captures non-linear relationships in spectral data while remaining robust to overfitting. The 2D-COS analysis proved especially valuable for feature selection, providing a chemically meaningful basis for focusing subsequent multivariate analysis [40].

Despite the promising classification performance, some of the drawbacks should be mentioned. This study uses a relatively small data set of 195 spectra collected from 70 kernels from a single research site. Stratified cross-validation and an independent test set have been used, but the small number of samples and geographical origin limit the generalizability of the results. The fungal species composition, distribution of DON, and matrix effects of natural Fusarium

infections may differ significantly as a result of wheat variety, environmental conditions, and agronomic practice. Hence, the current models should be considered proof of concept. Larger, multi-location, and multi-variety datasets are needed in the future to test the approach under conditions of reality.

### Assessment of method rapidity and turnaround time

The present study aimed to develop a rapid, non-destructive diagnostic tool for DON contamination. Consequently, the overall speed of the method was evaluated to determine the total time required to assess the infection status of a wheat kernel. Table *2* summarizes the estimated turnaround time for the complete Raman spectroscopy and machine learning pipeline.

| Phase | Activity | Time(minutes) |
|---|---|---|
| Sample preparation | Cleaning, sorting and longitudinal sectioning | <3 |
| Data acquisition | Raman spectra collection per kernel | <2 |
| Data analysis | Preprocessing, PCA, and classification | <3 |
| Overall time per kernel | | <8 |

**TABLE 2: Turnaround time for the machine learning-aided Raman spectroscopy method**

PCA, Principal Component Analysis

Compared to traditional confirmatory methods, such as ELISA (several hours) or GC-MS (over 60 minutes including extensive extraction and cleanup), the developed method allows a single kernel to be processed and classified within 8 minutes. This rapid turnaround validates the method's suitability for high-throughput screening and near-real-time decision support in grain inspection.

### Comparison with prior work

While our identification of these markers provides a foundation for DON detection, comparison with previous studies highlights the advantages of our methodological approach. Prior research has often relied on Surface-Enhanced Raman Spectroscopy (SERS) with complex substrate preparation, which introduces variability and limits practical deployment. For example, [19] applied SERS with silver nanoparticles to detect DON in agricultural products, achieving a low limit of detection for pure solutions but requiring multi-step synthesis and validation primarily on spiked rather than naturally infected grain. Similarly, the researchers [20] developed a SERS-based method using gold nanorods for DON detection in wheat, achieving 0.11 mg/L sensitivity, but their protocol involved complex nanoparticle synthesis, functionalization, and multi-step extraction procedures that are difficult to standardize for routine screening. The researchers [22] employed surface-enhanced Raman detection but noted challenges with spectral reproducibility and matrix interference, while [39] explored SERS using two-photon polymerized nanostructures, demonstrating signal enhancement at the cost of fabrication complexity. This study used naturally infected wheat kernels with minimal sample preparation, simple longitudinal sectioning, and conventional Raman spectroscopy, demonstrating that adequate sensitivity for DON classification (97-100% accuracy) can be achieved with conventional Raman when coupled with chemometric analysis.

## Conclusions

The results of this study successfully demonstrated that conventional Raman spectroscopy, 2D-COS, and machine learning are practical methods for rapid detection of DON contamination in wheat kernels. The method was used to identify and detect coordinated spectral changes related to DON and to use supervised classification models for high discrimination between healthy and infected samples. The overarching message of this work is that wheat kernel screening can be performed faster than traditional laboratory methods, such as ELISA or GC-MS, and thus can aid in making more prompt decisions on wheat quality assessment, especially in resource-constrained environments. The results obtained at this time, however, should be considered a proof of concept. More extensive field testing of more diverse samples is needed to validate the method prior to its routine use. The potential for whole kernel analysis without sectioning, the development of quantitative prediction models of DON concentration, and improvement of the generalizability of the model across wheat varieties and growing conditions should be explored as future efforts.

## Additional Information

### Author Contributions

All authors have reviewed the final version to be published and agreed to be accountable for all aspects of the work.

**Concept and design:** Antony M. Ngugi, Jared Ombiro Gwaro, Zennah C. Kosgey, Robinson Ndegwa

**Acquisition, analysis, or interpretation of data:** Antony M. Ngugi, Jared Ombiro Gwaro, Zennah C. Kosgey, Robinson Ndegwa

**Drafting of the manuscript:** Antony M. Ngugi, Jared Ombiro Gwaro, Zennah C. Kosgey, Robinson Ndegwa

**Critical review of the manuscript for important intellectual content:** Antony M. Ngugi, Jared Ombiro Gwaro, Zennah C. Kosgey, Robinson Ndegwa

**Supervision:** Antony M. Ngugi, Jared Ombiro Gwaro, Zennah C. Kosgey, Robinson Ndegwa

### Disclosures

**Plant subjects:** All authors have confirmed that this study did not involve any herbarium specimen. **Human subjects:** All authors have confirmed that this study did not involve human participants or tissue. **Animal subjects:** All authors have confirmed that this study did not involve animal subjects or tissue. **Conflicts of interest:** In compliance with the ICMJE uniform disclosure form, all authors declare the following: **Payment/services info:** All authors have declared that no financial support was received from any organization for the submitted work. **Financial relationships:** All authors have declared that they have no financial relationships at present or within the previous three years with any organizations that might have an interest in the submitted work. **Other relationships:** All authors have declared that there are no other relationships or activities that could appear to have influenced the submitted work.

### Data Availability Statements

The data (and/or code) supporting this study are openly available on https://github.com/TonyMuch76/Wheat-Analysis

### Acknowledgements

The completion of this research was made possible through the support and contributions of many individuals and institutions. Sincere gratitude is extended to the Kenya Agricultural and Livestock Research Organization (KALRO), Njoro, for providing the wheat samples used in this study. The University of Nairobi, Chiromo Campus, is gratefully acknowledged for offering laboratory facilities, equipment, and an enabling environment for the work. Special thanks are

due to the supervisors and technical staff at Chiromo Campus, whose guidance, assistance in data collection, and valuable feedback were instrumental throughout the research process. Deep appreciation is also expressed to family and friends for their unwavering moral support and understanding during the course of this academic journey.

## References

1. Alisaac E, Mahlein AK: Fusarium head blight on wheat: Biology, modern detection and diagnosis and integrated disease management. Toxins. 2023, 15:192. 10.3390/toxins15030192

2. Pestka JJ: Deoxynivalenol: mechanisms of action, human exposure, and toxicological relevance. Archives of Toxicology. 2010, 84:663-679. 10.1007/s00204-010-0579-8

3. U.S. Food and Drug Administration: Guidance for Industry and FDA: Advisory Levels for Deoxynivalenol (DON) in Finished Wheat Products for Human Consumption and Grains and Grain By-Products Used for Animal Feed. 2010,

4. Wagacha JM, Muthomi JW: Mycotoxin problem in Africa: Current status, implications to food safety and health and possible management strategies. International Journal of Food Microbiology. 2008, 124:1-12 . 10.1016/j.ijfoodmicro.2008.01.008

5. Zhang Z, Nie D, Fan K, et al.: A systematic review of plant-conjugated masked mycotoxins: Occurrence, toxicology, and metabolism. Critical Reviews in Food Science and Nutrition. 2019, 60:1523-1537. 10.1080/10408398.2019.1578944

6. Bai G, Shaner G: Management and resistance in wheat and barley to fusarium head blight. Annual Review of Phytopathology. 2004, 42:135-161. 10.1146/annurev.phyto.42.040803.140340

7. Beyer M, Klix MB, Verreet JA: Estimating mycotoxin contents of Fusarium-damaged winter wheat kernels. International Journal of Food Microbiology. 2007, 119:153-158. 10.1016/j.ijfoodmicro.2007.07.007

8. Njeru NK, Muthomi JW, Mutegi CK, Wagacha JM: Effect of cropping systems on accumulation of Fusarium head blight of wheat inocula in crop residues and soils. Journal of Plant Sciences. 2016, 11:12-21. 10.3923/jps.2016.12.21

9. Manley M: Near-infrared spectroscopy and hyperspectral imaging: non-destructive analysis of biological materials. Chemical Society Reviews. 2014, 43:8200-8214. 10.1039/c4cs00062e

10. Elmasry G, Kamruzzaman M, Sun DW, Allen P: Principles and applications of hyperspectral imaging in quality evaluation of agro-food products: a review. Critical Reviews in Food Science and Nutrition. 2012, 52:999-1023. 10.1080/10408398.2010.543495

11. Butler HJ, Ashton L, Bird B, et al.: Using Raman spectroscopy to characterize biological materials. Nature Protocols. 2016, 11:664-687. 10.1038/nprot.2016.036

12. Petersen M, Yu Z, Lu X: Application of Raman spectroscopic methods in food safety: a review. Biosensors. 2021, 11:187.

13. Kuhar N, Sil S, Verma T, Umapathy S: Challenges in application of Raman spectroscopy to biology and materials. RSC Advances. 2018, 8:25888-25908. 10.1039/c8ra04491k

14. Rohman A, Windarsih A, Lukitaningsih E, Rafi M, Betania K, Fadzillah NA: The use of FTIR and Raman spectroscopy in combination with chemometrics for analysis of biomolecules in biomedical fluids: A review. Biomedical Spectroscopy and Imaging. 2019, 8:55-71. 10.3233/bsi-200189

15. Ikedi RI, Birech Z, Kaniu MI: Rapid assessment of molasses adulterated honey using laser Raman spectroscopy and principal component analysis. Food Analytical Methods. 2023, 16: 1702-1710 .

16. Odongo KO, Kaniu MI, Ndung'u CN, et al.: Direct and rapid screening of calcium carbide in ripened bananas using chemometrics-assisted laser Raman spectroscopy. Applied Physics B. 2023, 129:84.

17. Egging V, Nguyen J, Kurouski D: Detection and identification of fungal infections in intact wheat and sorghum grain using a hand-held Raman spectrometer. Analytical Chemistry. 2018, 90:8616-8621. 10.1021/acs.analchem.8b01863

18. Moskovskiy MN, Sibirev AV, Gulyaev AA, et al.: Raman spectroscopy enables non-invasive identification of mycotoxins p. fusarium of winter wheat seeds. Photonics. 2021, 8:587. 10.3390/photonics8120587

19. Yuan J, Sun C, Guo X, et al.: A rapid Raman detection of deoxynivalenol in agricultural products. Food Chemistry. 2017, 221:797-802. 10.1016/j.foodchem.2016.11.101

20. Weng S, Hu X, Zhu W, et al.: Surface-enhanced Raman spectroscopy with gold nanorods modified by sodium citrate and liquid-liquid interface self-extraction for detection of deoxynivalenol in fusarium head blight-infected wheat kernels coupled with a fully

convolution network. Food Chemistry. 2021, 359: 129847.

21. Gabbitas A, Ahlborn G, Allen K, Pang S: Advancing mycotoxin detection: multivariate rapid analysis on corn using surface enhanced Raman spectroscopy (SERS). Toxins. 2023, 15:610. 10.3390/toxins15100610

22. Chen M, Su B, Huang J, Fu F, Dong Y: Surface-enhanced Raman detection of deoxynivalenol allenol in agricultural products. Chinese Journal of Chromatography. 2022, 40: 1039-1046.

23. Farber C, Sanchez L, Pant S, Scheuring D, Vales I, Mandadi K, Kurouski D: Potential of spatially offset raman spectroscopy for detection of zebra chip and potato virus y diseases of potatoes (Solanum tuberosum). ACS Agricultural Science & Technology. 2021, 1:211-221. 10.1021/acsagscitech.1c00024

24. Qiu M, Zheng S, Tang L, Hu X, Xu Q, Zheng L, Weng S: Raman spectroscopy and improved inception network for determination of fhb-infected wheat kernels. Foods. 2022, 11:578. 10.3390/foods11040578

25. Ndung'u CN, Kaduki KA, Kaniu MI, Kiruri LW: Enhanced detection of pesticide residues using two-dimensional Raman correlation spectroscopy and machine learning. Applied Spectroscopy Practica. 2024, 2:10.1177/27551857241303466

26. Kheseli OP, Imbahale SS, Okoth S, Otipa M, Wekesa VW: Prevalence and phylogenetic diversity of pathogenic fusarium species in genotypes of wheat seeds in three rift valley regions, Kenya. Advances in Agriculture . 2021, 2021:8839147. 10.1155/2021/8839147

27. Zhou H, Simmons CS, Sarntinoranont M, Subhash G: Raman spectroscopy methods to characterize the mechanical response of soft biomaterials. Biomacromolecules. 2020, 21:3485-3497. 10.1021/acs.biomac.0c00818

28. Guido R, Ferrisi S, Lofaro D, Conforti D: An overview on the advancements of support vector machine models in healthcare applications: A review. Information. 2024, 15:235. 10.3390/info15040235

29. Zhou W, Yan Z, Zhang L: A comparative study of 11 non-linear regression models highlighting autoencoder, DBN, and SVR, enhanced by SHAP importance analysis in soybean branching prediction. Scientific Reports. 2024, 14:5905. 10.1038/s41598-024-55243-x

30. Breiman L: Random forests. Machine Learning. 2001, 45:5-32. 10.1023/a:1010933404324

31. Cortes C, Vapnik V: Support-vector networks. Machine Learning. 1995, 20:273-297. 10.1007/bf00994018

32. Schölkopf B, Smola AJ: Learning with Kernels: Support Vector Machines, Regularization, Optimization, and Beyond. MIT Press, London; 2002.

33. Erickson BJ, Kitamura F: Magician's Corner 9. performance metrics for machine learning models. Radiology: Artificial Intelligence. 2021, 3:e200126. 10.1148/ryai.2021200126

34. Rainio O, Teuho J, Klén R: Evaluation metrics and statistical tests for machine learning. Scientific Reports. 2024, 14:6086. 10.1038/s41598-024-56706-x

35. Vujovic Z: Classification model evaluation metrics. International Journal of Advanced Computer Science and Applications. 2021, 12:10.14569/ijacsa.2021.0120670

36. Rodriguez RS, Szlag VM, Reineke TM, Haynes CL: Multiplex surface-enhanced Raman scattering detection of deoxynivalenol and ochratoxin A with a linear polymer affinity agent. Materials Advances. 2020, 1:3256-3266. 10.1039/d0ma00608d

37. Ozaki Y, Šašic S, Tanaka T, Noda I: Two-dimensional correlation spectroscopy: Principle and recent theoretical development. Bulletin of the Chemical Society of Japan. 2001, 74:1-17. 10.1246/bcsj.74.1

38. Noda I: Two-dimensional correlation analysis useful for spectroscopy, chromatography, and other analytical measurements. Analytical Sciences. 2007, 23:139-146. 10.2116/analsci.23.139

39. Liu Q, Vanmol K, Lycke S, Van Erps J, Vandenabeele P, Thienpont H, Ottevaere H: SERS using two-photon polymerized nanostructures for mycotoxin detection. RSC Advances. 2020, 10:14274-14282. 10.1039/ D0RA01915A

40. Thuku JM, Kaniu MI, Ndung'u CN, Kiruri LW, Kaduki KA: Rapid trace detection of chlorpyrifos in vegetables using 2D Raman correlation spectroscopy and machine learning. LWT. 2025, 237:118742. 10.1016/j.lwt.2025.118742

41. Bro R, Smilde AK: Principal component analysis. Analytical Methods. 2014, 6:2812-2831. 10.1039/c3ay41907j

**How to cite this article:**
Ngugi A M, Kosgey Z C, Ndegwa R, et al. (September 02, 2026) Rapid Detection of Deoxynivalenol in Wheat Using 2D Raman Correlation Spectroscopy and Machine Learning. Cureus J. Agri. Food Sci 2 : es44497-026-00258-7. DOI https://doi.org/10.7759/s44497-026-00258-7